Accepted Manuscript

An alternative fluorine precursor for the synthesis of SnO_2:F by spray pyrolysis

E. Arca, K. Fleischer, I.V. Shvets

PII: S0040-6090(11)01645-2
DOI: doi: 10.1016/j.tsf.2011.09.016
Reference: TSF 29811

To appear in: *Thin Solid Films*

Received date: 10 January 2011
Revised date: 2 September 2011
Accepted date: 8 September 2011

Please cite this article as: E. Arca, K. Fleischer, I.V. Shvets, An alternative fluorine precursor for the synthesis of SnO_2:F by spray pyrolysis, *Thin Solid Films* (2011), doi: 10.1016/j.tsf.2011.09.016

This is a PDF file of an unedited manuscript that has been accepted for publication. As a service to our customers we are providing this early version of the manuscript. The manuscript will undergo copyediting, typesetting, and review of the resulting proof before it is published in its final form. Please note that during the production process errors may be discovered which could affect the content, and all legal disclaimers that apply to the journal pertain.

ACCEPTED MANUSCRIPT

An alternative fluorine precursor for the synthesis of SnO_2:F by spray pyrolysis

E. Arca[1*], K. Fleischer[1], and I. V. Shvets[1]

[1]Cleaner Energy Laboratory, School of Physics, Trinity College Dublin, Dublin 2, Ireland

ACCEPTED MANUSCRIPT

[*] Corresponding author: earca@tcd.ie, Ph: +353 (0)1 896 3808

ACCEPTED MANUSCRIPT

Abstract

An alternative, non-toxic precursor was employed for the synthesis of SnO_2:F transparent conducting oxide. The performance of benzenesulfonyl fluoride (BSF) as F source for spray pyrolysis was investigated. Its decomposition and the actual incorporation of fluorine in the tin oxide matrix were confirmed by X-ray photoelectron spectroscopy while its effect on the electrical properties was investigated by resistance and Hall measurements. Results were compared with respect to samples grown using a common fluorine source (NH_4F), a commercial available sample and a sample grown by spray pyrolysis at an independent laboratory. We show that BSF leads to actively doped conductive SnO_2 with good carrier mobility, though the fluorine incorporation rate and hence overall conductivity of the films is lower than for fluorine precursors commonly used in spray pyrolysis.

Key-words: Fluorinated Tin Oxide (SnO_2:F), Transparent Conductive Oxide (TCO), fluorine source, spray-pyrolysis

ACCEPTED MANUSCRIPT

ACCEPTED MANUSCRIPT

Introduction

Transparent conducting oxides (TCO) are becoming increasingly important as critical components of a variety of thin film technologies such as smart windows, flat panel display and solar cells. This is mainly due to the coexistence of both high transparency to light in the visible region and high conductivity, with values comparable to those of metals. In particular thin film solar cells have shown high market growth (30% per year) in recent years and will continue playing an important role in minimising the cost of photovoltaic power generation. Two of the most important thin film technologies, namely a-Si and CdTe solar cells, use a TCO as the first layer in the stack. In order to be implemented in a solar cell, a TCO should be highly transparent in the visible range (transmittance≥80%), and highly conductive (R_{sh} ≤10 Ω/□). [1, 2] Moreover, in order to be implemented in a large scale production, the material of the TCO should be abundant, low cost and, if possible, environmental friendly. Among the different TCOs available, fluorinated tin oxide (SnO_2:F or FTO) can fulfil most of these requirements. In fact tin oxide is a transparent conductive oxide even in its undoped state. The conductivity is due to an intrinsic non-stoichiometry, created by the presence of oxygen vacancies (V_o) and interstitial tin (Sn_i) inside the structure, which are easily tolerated due to the multivalence of tin [3, 4]. Spontaneous acceptor-like intrinsic defects, like interstitial oxygen or tin vacancies are absent, therefore the electrons released by the V_o or Sn_i are not compensated. Transparency, instead, is a consequence of the large gap between the top of the valence band and the first unoccupied state, so that direct optical transitions in the visible range are not allowed. In this way, it is possible to have a simultaneous high carrier concentration with minor effects on transparency [3]. However, in order to further improve the conductivity, tin oxide is generally doped, either with Sb or F [5-7] as substitutes for tin and oxygen respectively. Due to differences in the valence state and in hybrid orbital configuration in both cases a free electron is released if one of these two doping atoms is

ACCEPTED MANUSCRIPT

present. However, F is normally preferred to Sb because, at high doping concentration, a reduction in the mobility and lower transparency has been observed for Sb doped films.[6-8]. For these reasons FTO is a widely used TCO in both CdTe and amorphous silicon based solar cells [1]. The best commercial FTO (Ashai U-type) shows a transparency of 80% in the visible range and a resistivity of 1.4 $10^{-5}\Omega$cm [2]. Although extensively used in research laboratories, this product is not yet ready for a large scale industrial application [2]. Therefore, deposition of FTO is still being studied in order to achieve good quality and low cost.

On a laboratory scale, SnO_2-based films are grown with wide range of deposition techniques such as sputtering, sol-gel, and various chemical vapour deposition (CVD) techniques [9, 10]. For the TCO growth in the photovoltaic sector only sputtering and CVD variants (in particular plasma enhanced CDV) are in widespread use due to their cost efficiency and scalability. It is well known that widespread use of solar cells will only be possible if abundant, non-toxic materials are used and if a fast, inexpensive and scalable technique is available for the deposition. Spray pyrolysis could fulfil these requirements, providing films with optical and electrical properties comparable with those grown by the more expensive vacuum deposition techniques currently used. [11-14]

For a long time $CBrF_3$ has been used as F source for CVD. However this is a greenhouse gas which has been gradually phased out from the market [15]. Thus an alternative fluorine source is needed. For this reason either HF or NH_4F have been often reported as F source in spray pyrolysis and other CVD techniques [6, 7, 16]. However both of them are classified as toxic.

In this work an attempt has been made to find an alternative, non-toxic precursors to grow SnO_2:F with performances comparable to those of films prepared with the conventional precursors. For this purpose benzenesulfonyl fluoride (BSF) has been tested as F source. Electrical and optical properties of the films have been compared to those of samples grown using NH_4F, to a commercial SnO_2:F

ACCEPTED MANUSCRIPT

(Solaronix Switzerland) which will be addressed as REF-1 from here after, and also to a sample grown by spray pyrolysis provided by an independent group which will be addressed as REF-2 [13].

Experimental details

Samples have been grown by spray pyrolysis, using a compressed gas spray system in a custom build chamber using a fast responsive AlN heater. Details of the system are described elsewhere [17].

As with any CVD technique actual growth rates or dopant incorporation rates crucially depend on substrate temperature, precursor concentration and in case of spray pyrolysis also the solvent [11, 17]. Hence for every precursor growth parameters have been individually optimised and currently best performing samples are compared. Two different precursors have been used as tin sources (dibutyltin diacetate (DBTDA) and tin chloride pentahydrate ($SnCl_4{\cdot}5H_2O$)). Ammonium fluoride (NH_4F) and benzenesulfonyl fluoride were used as fluorine source. For both fluorine precursors, different Sn:F ratios (at.%) were investigated, namely 50:50, 67:37, 80:20, 91:9. The best decomposition temperature was found in range 450-480ºC.

For DBTDA and $SnCl_4{\cdot}5H_2O$ a 0.1M solution has been prepared using methanol or ethanol as solvent. It was experimentally verified that film quality was not affected by the choice of either one of the two solvents. Methanol is less expensive, however ethanol is not toxic. The deposition temperature was screened over a range spreading from 420ºC to 500ºC in steps of 10ºC for each precursor. Best performing samples have been grown using $SnCl_4{\cdot}5H_2O$ at 480ºC. When DBTDA was used, the nozzle was allowed to scan laterally in order to improve the homogeneity of the deposition. The scanning amplitude was restricted to $\pm$ 0.02 m. Moreover when $SnCl_4{\cdot}5H_2O$ was used as a Sn source, discontinuous growth provided better samples: in this case, every 2 minutes, the spraying was switched off and the sample was annealed for 2 minutes. However the overall time of spraying, and thus the amount of material used for the deposition, was the same as in the continuous growths. Deposition time

ACCEPTED MANUSCRIPT

was set to 10 minutes. Due to different precursors used as tin source, thickness values range from 500 to 700 nm, with higher growth rate for tin chloride. The thickness of each sample was measured optically after the growth (see below).

Microscope glass slides (Fisher brand, thickness 0.8-1 mm) or cover slips (Roth, thickness 0.17 mm) were used as substrates. The actual composition of each sample was investigated by X-ray photoelectron spectroscopy (XPS) using an Omicron MultiprobeXP system (Mg X-ray source, E125 Analyser). Samples have been cleaned in-situ using 5min of Ar ion sputtering at 3×10^{-4} Pa, 1.5 kV beam energy and an ion target current of 6μA using an Omicron ISE 5 cold cathode ion sputter source. Experimental data were analyzed using the CasaXPS software.

Optical properties were investigated by UV-Vis spectrophotometry and spectroscopic ellipsometry (SE). In the former case a Cary 50 UV-Vis-NIR-spectrophotometer equipped with a Xenon lamp was used. For the SE analysis, a SOPRA GESP 5 Variable Angle spectroscopic ellipsometer was used in the energy range from 1.5 to 5 eV, at three different angles of incidence (ϕ = 55°, 60°, 65°). Multiple angles measurements are required in order to decouple the correlation between the refractive index (n) and the thickness of the sample (d). Experimental data were fitted using a multilayer model consisting of air, a rough surface area, the thin film and glass. The line-shape of the dielectric function of the film was reconstructing using a three dimensional critical point [18]. The parameters associated with it (amplitude of the critical point, the threshold energy, the broadening and the excitonic phase angle) as well as the thickness of the sample were introduce as a variable, whose values were optimized via an iterative fitting procedure with respect to the raw ellipsometric data at multiple angles. To further confirm the validity of the data acquired in this way, transmission measurements were analysed, using database refractive indices for FTO. The thickness values determined via the ellipsometric model and via spectrophotometry coincide within the experimental error (±20 nm).

ACCEPTED MANUSCRIPT

Electrical properties were investigated in standard 4 point probe square geometry. Due to the previously mentioned differences in the growth rates for different precursors, film thickness varied between samples. Therefore we are going to compare resistivity values, not the sheet resistance using the optically determined thickness value of each sample. Selected samples were also subjected to Hall measurement in order to determine both mobility and bulk carrier density. Colloidal silver paint was used to provide ohmic contacts. The same system was used to investigate the dependence of the sheet resistance on temperature in a range from 70 to 300 K, allowing the determination of the activation energy for the carriers.

Results and Discussion

In order to confirm that the alternative precursor does not alter the optical properties of the FTO films, the line shape of the dielectric function and the optical band gap were determined by spectroscopic ellipsometry. Their values were further confirmed by fitting the UV-Visible transmission data (Figure 1). Within the experimental error, the dielectric function of all the samples was found to be the same. No significant difference was found regarding the band gap of both NH_4F and BSF grown sample, as well as in comparison to REF-1 and REF-2, although it is worth noting that, in comparison to the undoped sample, all those doped with fluorine show the expected band gap opening due to Burnstein-Moss effect. Nevertheless differences in specular transmission could be found even for sample grown using the same fluorine source, due to different scattering loss (haze). Haze turns out to be caused by the roughness at the surface, whose value depends on both the precursor used as tin source and deposition temperature. In particular chloride introduces more roughness with respect to DBTDA.

Best room temperature resistivities for samples grown using NH_4F as fluorine source were found to be $1.4 \cdot 10^{-3}$ Ωcm and $1.6 \cdot 10^{-3}$ Ωcm with $SnCl_4 \cdot 5H_2O$ and DBTDA as Sn precursor respectively. These

ACCEPTED MANUSCRIPT

values are below those of REF-1 ($5\cdot10^{-4}$ Ωcm) and REF-2 ($6\cdot10^{-4}$ Ωcm) but in accordance to other spray pyrolysis grown FTO films [19, 20].

In the main experiment, the alternative fluorine source (BSF) was tested. In this case a screening of different temperature and ratio Sn:F has been carried out, but, again, only representative samples will be presented. Taking into consideration the resistivity, the best condition for the deposition was found to be 480ºC with a Sn:F ratio of 50:50. In this condition a minimum resistivity of 4.3 10^{-3} Ωcm has been found using $SnCl_4\cdot5H_2O$ as tin source. Compared to the undoped sample grown under the same conditions, this corresponds to an improvement of 50% in the conductance. The actual incorporation of fluorine was confirmed by XPS. As shown in Figure 2, for all samples it is possible to identify the F 1s peak at the characteristic binding energy around 685 eV [21].

At this time no quantitative analysis of the F incorporation is possible for various reasons. Due to the surface sensitivity of the XPS measurements the presence of F in as-grown samples is not a sufficient indication of fluorine incorporation. There is the possibility that the surface is contaminated by precursor solution residue, which contains fluorine. Therefore Argon ion sputtering of 1.5kV Ar ions for 5 min has been employed to remove residual carbon and other potential contaminants from the precursor solution (see Figure 3). Unfortunately the Ar sputtering treatment changes the surface composition and roughness as lighter elements such as O and F are preferably removed. Figure 3 shows the effect of the cleaning cycles on the relative intensities of the Sn 3d, O 1s and F 1s core levels for sample REF-1 with the highest F concentration and lowest initial carbon contamination of all investigated samples. It is evident, that the cleaning does change the measured Sn/F and Sn/O ratios indicating a change in the stoichiometry of the surface area of the oxide, or the removal of precursor residuals. Nevertheless after sputtering the presence of F has been confirmed for both fluorine precursors and measured Sn/F ratios scale with the carrier concentration of the samples (see inset Figure 2). This indicates that the measured fluorine after sputtering originates from incorporated

ACCEPTED MANUSCRIPT

fluorine, even if the measured absolute values of the F/Sn ratios are not indicative of the real fluorine content in the SnO_2 matrix. It is also worth noting, that measurement times were limited, as extensive exposure of all samples to the Al Kα X-rays (>1h) lead to a steady decline in the detected fluorine signal.

Resistance measurement have been carried out over a set of samples grown under the same conditions but with different nominal Sn:F ratio. While all the other samples show a characteristic metallic behaviour in resistance vs. temperature plot, the samples grown using BSF show a metallic behaviour at high temperature while at lower temperatures the resistance increases again, as expected for semiconductors (Figure 4 and 5). This suggests that more than one type of carrier contributes to the overall conductance and there is still a large contribution of these intrinsic carriers to the measured total conductance. The temperature, at which this transition occurs (here defined as a change in slope), is a function of BSF concentration (Figure 5). When the nominal atomic ratio Sn:F is 1, incorporation is good enough to lead to a metallic behaviour almost in the whole range of temperature. As the nominal concentration of fluorine decreases, the transition temperature shifts to higher values.

Samples grown using the alternative precursors show a lower carrier concentration compared to all the other samples (Table 1). However, the mobility of the carriers is comparable to those found for REF-1 and REF-2 and it is much higher than in samples grown using NH_4F as precursor. At present it is not clear, whether the lower carrier concentration in BSF grown films is related to a lower efficiency in the decomposition process of BSF itself or is due to a lower incorporation rate of the fluorine atoms or alternative fluorine could be partly passivated by compensating defects introduced by C, S, or H also present in the precursor. However as the measured fluorine concentration scales well with measured carrier concentration (see inset Figure 2), a lower incorporation rate is more likely.

Several scattering mechanisms might influence the mobility of the carriers [6-8]. Among them, the key mechanisms are scattering due to neutral impurities, due to ionized impurities, due to phonon and

ACCEPTED MANUSCRIPT

scattering at grain boundaries. Each of these single mechanisms contributes to the total mobility of the carriers; however, the extent of the contribution can be considerably different and might be confined only to specific temperature region. For example, in a heavily doped semiconductor contribution of neutral impurities can be neglected taking into consideration that even at rather low temperature (77K) their concentration is really low as most of impurities are fully ionized [8].

In the case of non degenerated semiconductors where carriers are scattered by ionized impurities, mobility depends on temperature as $\mu \propto T^{3/2}$. For degenerate semiconductors, instead, mobility is independent of temperature and it can be calculated according to the Brooks-Herring formula:

$$\mu_{IID} = \left(\frac{2}{m^*}\right)^{1/2} \frac{\varepsilon^2 E_F^{3/2}}{\pi\, e^3 f(x) N_i} \tag{1}$$

Being m^* the reduced mass whose value was takes as $0.3m$, m the electron mass, e is the electron charge, ε the absolute dielectric permittivity, E_F the Fermi level, N_i the density of scattering centres which is taken equal to the number of carriers and $f(x)$ a function of the screen radius r_s as follows:

$$f(x) = \ln(1+x) - \frac{x}{1+x} \tag{2}$$

$$x = \frac{8m^* E_F r_S^2}{\hbar^2} \tag{3}$$

$$r_S = \frac{\hbar}{2e}\left(\frac{\varepsilon}{m^*}\right)^{1/2}\left(\frac{\pi}{3N_i}\right)^{1/6} \tag{4}$$

where $\hbar$ is the Planck constant.

Optical phonons are energetic modes therefore their contribution to scattering of electrons at room temperature can be neglected [22]. Scattering due to acoustical phonons will be characterized by a dependence of carriers mobility on temperature as $AT^{-3/2}$ according to the following equation: [7, 8].

$$\mu_L = \frac{(8\pi)^{1/2} e\hbar^4 C_{ii}}{3E_I^2 (m^*)^{5/2} (kT)^{3/2}} \tag{5}$$

ACCEPTED MANUSCRIPT

$$E_I = V\left(\frac{dT}{dV}\right)\left(\frac{dE_g}{dT}\right) \quad (6)$$

However determining the mobility value by using this formula is not possible as, currently no data are available for the value of the elastic constant for longitudinal waves C_{ii} and for the volume expansion coefficient $\left(\frac{1}{V}\frac{dV}{dT}\right)$.

Mobility limitation due to grain boundaries can be determined according to the following equation:

$$\mu_{GB} = le\left(\frac{1}{2\pi m^* kT}\right)^{1/2} \exp\left(\frac{-E_a}{kT}\right) \quad (7)$$

Where E_a is the activation energy and l is the grain size.

It is worth noting that all of these formulas are valid under the assumption that a single type of carrier is present. This is not the case for the fluorinated tin oxide. In fact, as previously reported, the undoped samples are already conductive and therefore more than one type of defects can be the source of conductivity in doped samples.

For samples grown using BSF, the commercial and the independent samples, the principal scattering mechanism is due to acoustical phonons in the temperature range of 300-150K and ionized impurities for temperature lower than 150K. This conclusion has been drawn by taking into consideration the dependence of the mobility as a function of temperature (Figure 6 and 7). A linear dependence of mobility vs. $T^{-3/2}$ is present down to a temperature of 200K (Figure 7, equation (5)). Therefore it can be argued that the principal scattering mechanism in this temperature range is due to phonons. Below this value the mobility becomes independent of the temperature down to a value of 70K, meaning that phonons are frozen in and ionized impurities represent the principle scattering mechanism in this region (Figure 6, equation (1)). Either way, both mechanisms are intrinsic to the material itself and cannot be suppressed. This means that the only way to improve the material conductivity is by increasing the carrier concentration. However, this is not recommended for the samples provided by the independent

ACCEPTED MANUSCRIPT

laboratory and the commercial one, as increasing the carrier density would push up the Drude tail in the visible range, thus compromising the optical properties of the materials. In other words, once the optimum carrier concentration is reached and the scattering mechanisms are only intrinsic, improving the material is not possible any longer.

Samples grown employing NH_4F show a much lower mobility compared to BSF grown samples but the overall shape of the curve is consistent with the previous picture (see also Table 1). This means that again phonons play an important role up to 200 K while below this temperature, ionized impurities become relevant. In this case, in order to account for the lower mobility, a third mechanism has also to be considered: grain boundary. As stated before, grain boundaries are not an intrinsic limitation to the mobility, therefore there are prospects for improving the electrical properties. One possible avenue for this is a post growth annealing, which was shown to improve the material performance [23]. Preliminary studies using in vacuum annealing however did not improve the samples, on the contrary the resistivity and carrier mobility decreased after the process. As a result, further studies to determine the optimum annealing condition and the difference in measured mobilities for the two fluorine sources are required.

ACCEPTED MANUSCRIPT

Conclusion

An alternative precursor has been tested as fluorine source for the synthesis of SnO_2:F by spray pyrolysis. Its performance has been compared to a commonly used source, NH_4F. Incorporation of fluorine has been indirectly shown by the improvement in conductivity and directly by identification of the fluorine 1s core level in XPS measurements.

Tin oxide produced using BSF has higher resistivity than those obtained by using NH_4F. The reason for this is likely to be a lower decomposition or incorporation efficiency of BSF which results in a lower carrier concentration in the samples. Instead, the Hall mobility of samples using BSF is

ACCEPTED MANUSCRIPT

comparable to those of the commercial and independent laboratory samples, indicating that the typical low mobility found for spray pyrolysis grown, untreated FTO is caused by the use of NH_4F, and not the deposition technique itself. For all investigated FTO samples phonon scattering represents the principal scattering mechanism in the region between 300 K and 200 K, while at lower temperature, scattering by ionized impurities dominates. When NH_4F was used, instead, scattering due to grain boundaries also contributes to limiting the mobility.

Acknowledgment

The authors would like to acknowledge financial support from Enterprise Ireland under grant PC/2007/0367.

ACCEPTED MANUSCRIPT

ACCEPTED MANUSCRIPT

Sample	carrier concentration (cm^{-3})	Hall mobility ($cm^2V^{-1}s^{-1}$)	Growth temperature (°C)	Sn precursor
SnO_2:F BSF (0.5)	$5 \cdot 10^{+19}$	28	480	$SnCl_4$
SnO_2:F BSF (1.0)	$6.6 \cdot 10^{+19}$	31	480	$SnCl_4$
SnO_2:F NH_4F	$4 \cdot 10^{+20}$	10	480	$SnCl_4$
REF-2	$3.5 \cdot 10^{+20}$	32		
REF-1	$5 \cdot 10^{+20}$	30		

Table 1: Room temperature electrical characteristics and growth conditions of representative samples, used for the XPS analysis.

ACCEPTED MANUSCRIPT

ACCEPTED MANUSCRIPT

Figure 1 Example of the ellipsometric analysis carried out on the samples: A) measured ellipsometric data (□) and modelled (—); B) refractive index n (—) and extinction coefficient k (**---**) as derived from A; C) comparison of the experimental UV-Vis data (---) with respect to the expected transmittance (—) for a layer with the same thickness and dielectric function derived from the ellipsometric model (B).

Figure 2 XPS on different tin oxide samples in the F 1s and Sn 3p 3/2 region. The inset shows the correlation between measured carrier concentration and F/Sn ratio derived from the XPS analysis.

Figure 3 XPS of sample REF-1 showing the effect of the 5 min surface cleaning employed for all samples. The C 1s, Sn 3d, O 1s, F 1s and Sn 3p 3/2 region are shown

Figure 4 Arrhenius plot of resistivity versus reciprocal temperature for samples showing a typical metallic behaviour (SnO_2:F NH_4F: —**,** REF-1: ····). As the resistivity value of our sample is higher, different range of scales are used. The inset compares the results sample REF-1 and REF-2 (– –).

Figure 5 Resistivity vs reciprocal temperature for a set of samples grown using BSF as fluorine source and varying Sn:F ratio in solution: (— 91:9, — 80:20, — 67:33, — 50:50). An offset equal to $\ln(\rho_{min})$ was subtracted to emphasize the change from a behaviour dominated by the metal like carriers to a semiconducting one. The inset shows the dependence of the temperature of transition from metallic to semiconductor behaviour (■) and absolute resistivity (○) on the nominal F:Sn ratios.

ACCEPTED MANUSCRIPT

ACCEPTED MANUSCRIPT

Figure 6: Exemplary Hall mobility vs temperature data for REF-1. The line shape of the curve is representative for all samples investigated, although absolute values vary.

Figure 7: Power dependence of the mobility values upon temperature shows that in the range between 300 and 150 K, the mobility $\mu^{-2/3}$ varies linearly with temperature. Below 150 K mobility becomes independent of temperature.

References

[1] D.W. Sheel, H.M. Yates, P. Evans, U. Dagkaldiran, A. Gordijn, F. Finger, Z. Remes, M. Vanecek, Thin Solid Films 517 (2009) 3061.
[2] J. Loffler, Ph.D. Thesis, Faculteit Natuuren Sterrrenkunde, Universiteit Utrecht, The Netherlands, 2005.
[3] A.K. Singh, A. Janotti, M. Scheffler, C.G. Van de Walle, Phys. Rev. Lett. 101 (2008) 055502.
[4] C. Kilic, A. Zunger, Phys. Rev. Lett. 88 (2002) 095501.
[5] J. Sun, A.X. Lu, L.P. Wang, Y. Hu, Q. Wan, Nanotechnology. 20 (2009) 335204.
[6] E. Elangovan, M.P. Singh, K. Ramamurthi, Mater. Sci. Eng. B 113 (2004) 143.
[7] K.S. Ramaiah, V.S. Raja, Appl. Surf. Sci. 253 (2006) 1451.
[8] B. Thangaraju, Thin Solid Films 402 (2002) 71.
[9] A. Facchetti, T.J. Marks, Transparent electronics: from synthesis to applications, Wiley, Oxford, 2010.
[10] C.G. Granqvist, Sol. Energ. Mater. Sol. Cells 91 (2007) 1529.
[11] P.S. Patil, Mater. Chem. Phys. 59 (1999) 185.
[12] K.S. Shamala, L.C.S. Murthy, K.N. Rao, B. Mater. Sci. 27 (2004) 295.
[13] K. Murakami, K. Nakajima, S. Kaneko, Thin Solid Films 515 (2007) 8632.
[14] S. Aukkaravittayapun, N. Wongtida, T. Kasecwatin, S. Charojrochkul, K. Unnanon, P. Chindaudom, Thin Solid Films 496 (2006) 117.
[15] M.B. Xiaonan Li, Joel Pankow, Sally E. Asher, Helio Moutinho, and, T. Gessert, Mater. Res. Soc. Symp. Proc 1012 (2007) 51.
[16] Z.B. Zhou, R.Q. Cui, G.M. Hadi, W.Y. Li, Z.M. Ding, J. Mater. Sci.-Mater. Electron. 12 (2001) 417.
[17] E. Arca, K. Fleischer, I.V. Shvets, J. Phys. Chem. C 113 (2009) 21074.
[18] P. Lautenschlager, M. Garriga, M. Cardona, Phys. Rev. B 36 (1987) 4813.
[19] A.I. Martinez, L. Huerta, J.M.O.R. de Leon, D. Acosta, O. Malik, M. Aguilar, J. Phys. D 39 (2006) 5091.
[20] M. Oshima, K. Yoshino, J. Electron. Mater. 39 (2010) 819.
[21] D. Briggs, Handbook of X-ray and ultraviolet photoelectron spectroscopy, Heyden, London, 1977.
[22] P.Y. Yu, M. Cardona, Fundamentals of Semiconductors, Physics and Materials Properties, Springer, Berlin Heidelberg, 1999.
[23] E. Shanthi, A. Banerjee, V. Dutta, K.L. Chopra, Thin Solid Films 71 (1980) 237.

ACCEPTED MANUSCRIPT

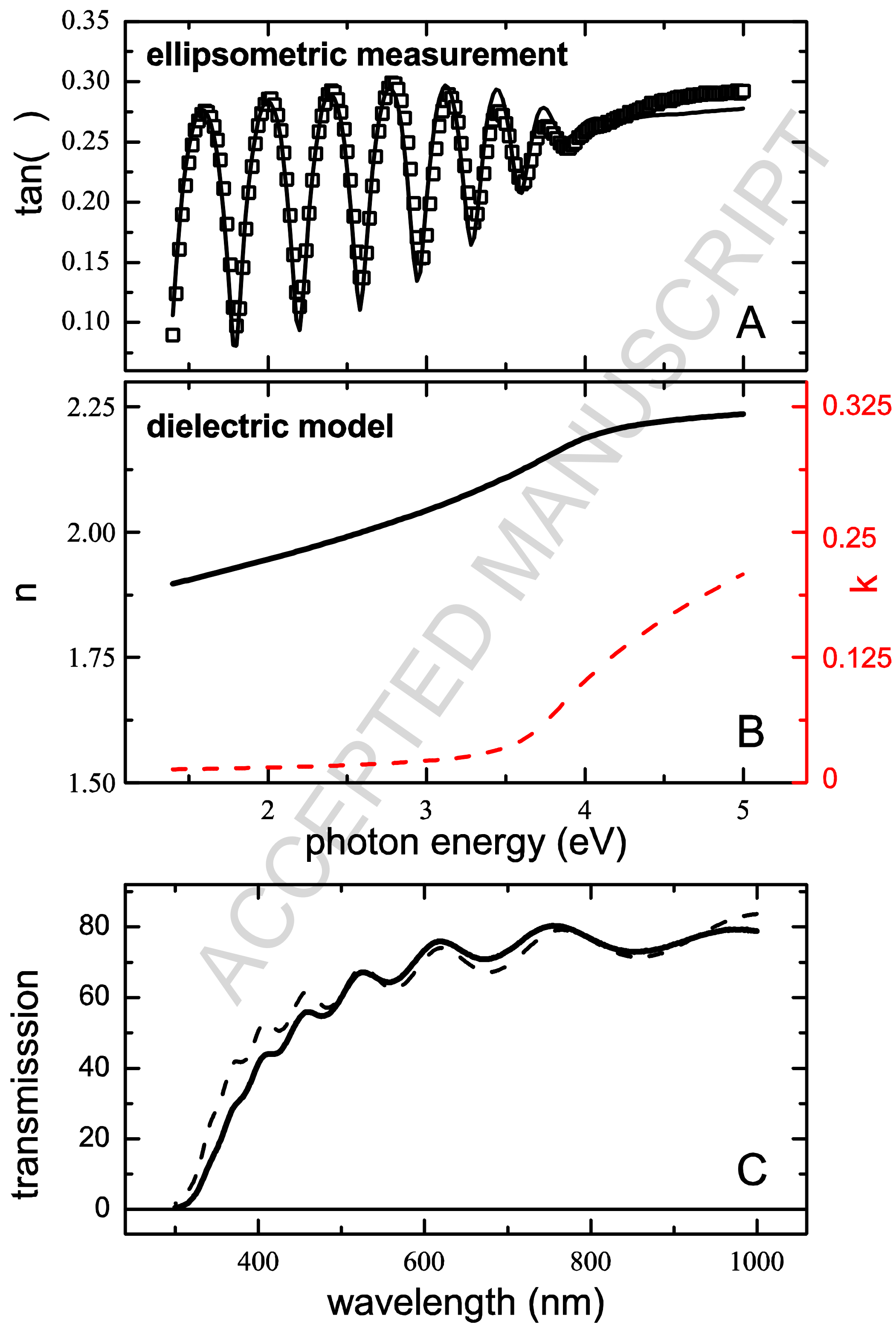

Fig. 1

ACCEPTED MANUSCRIPT

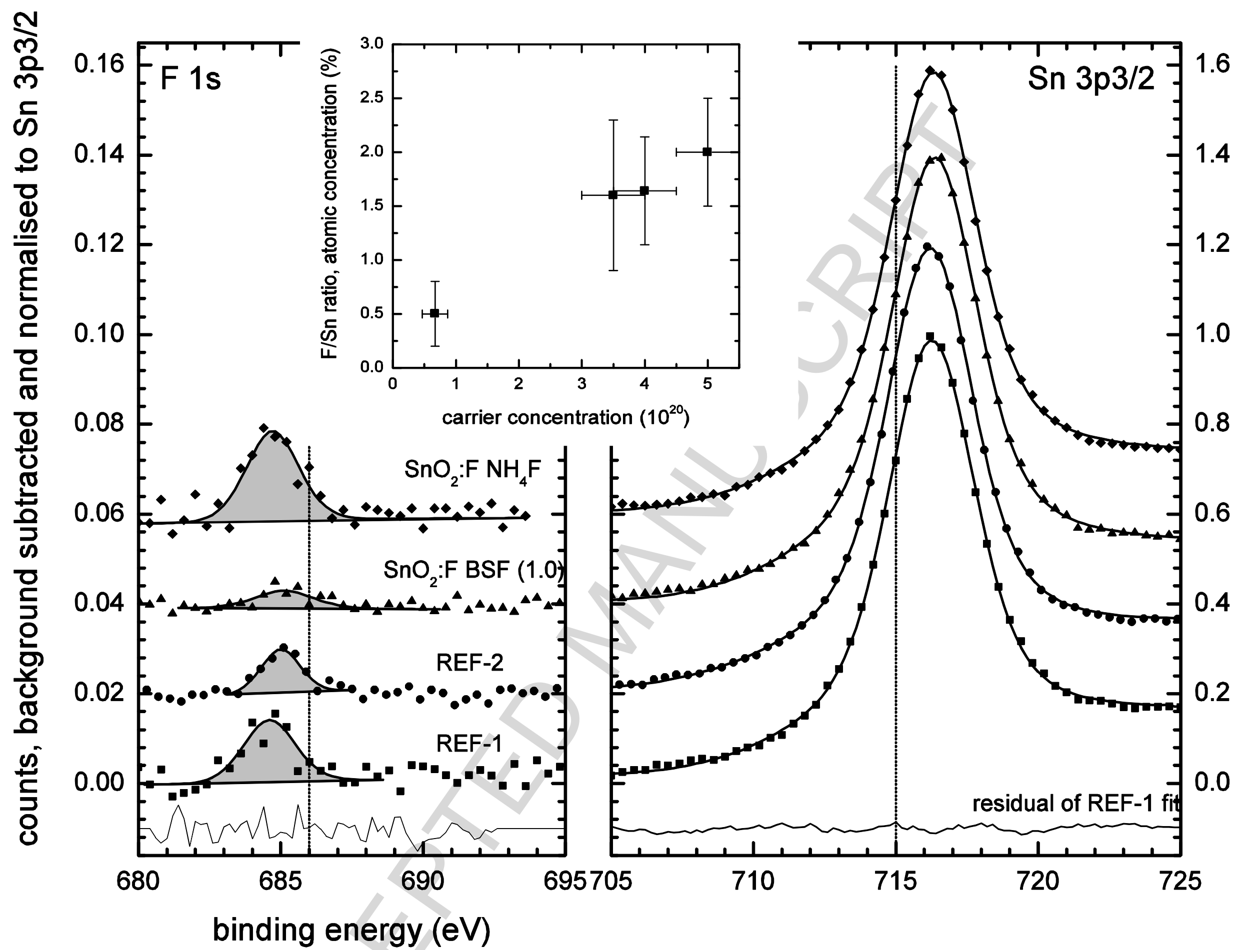

Fig. 2

ACCEPTED MANUSCRIPT

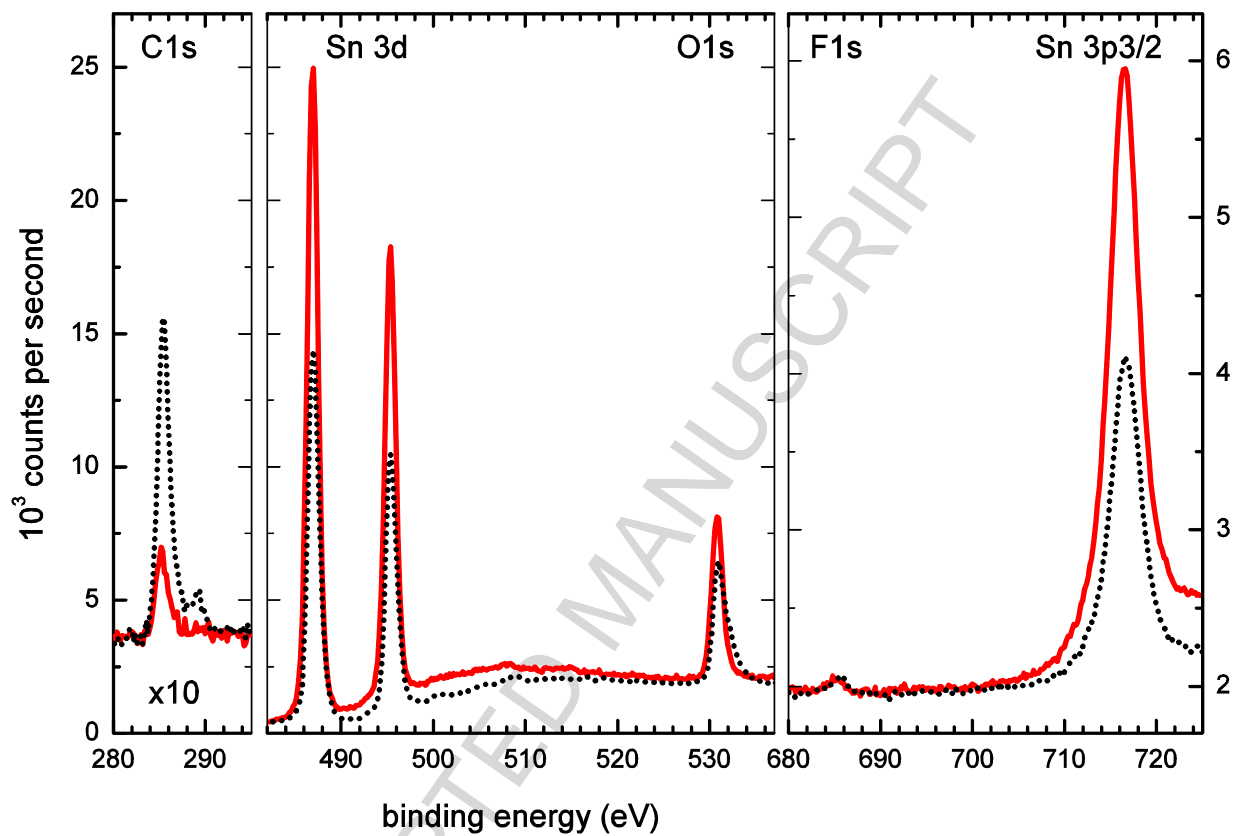

Fig. 3

ACCEPTED MANUSCRIPT

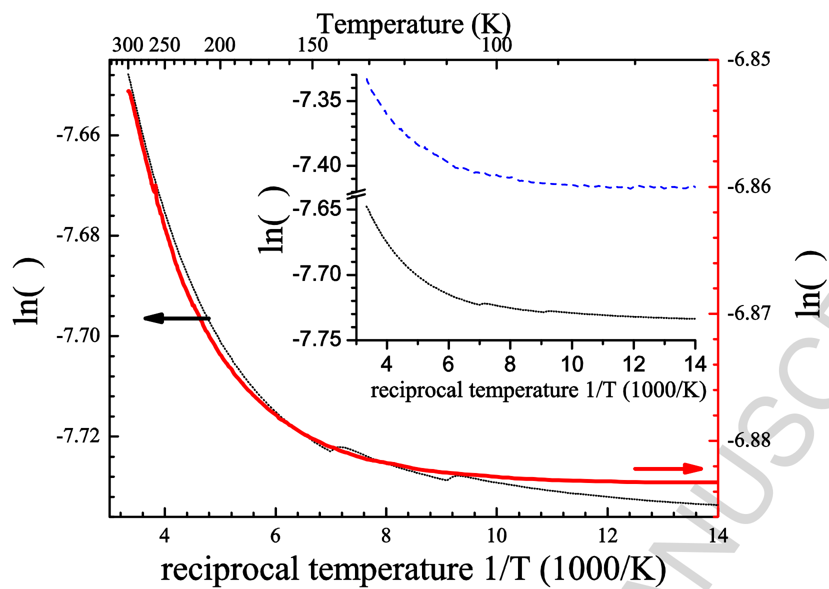

Fig. 4

ACCEPTED MANUSCRIPT

ACCEPTED MANUSCRIPT

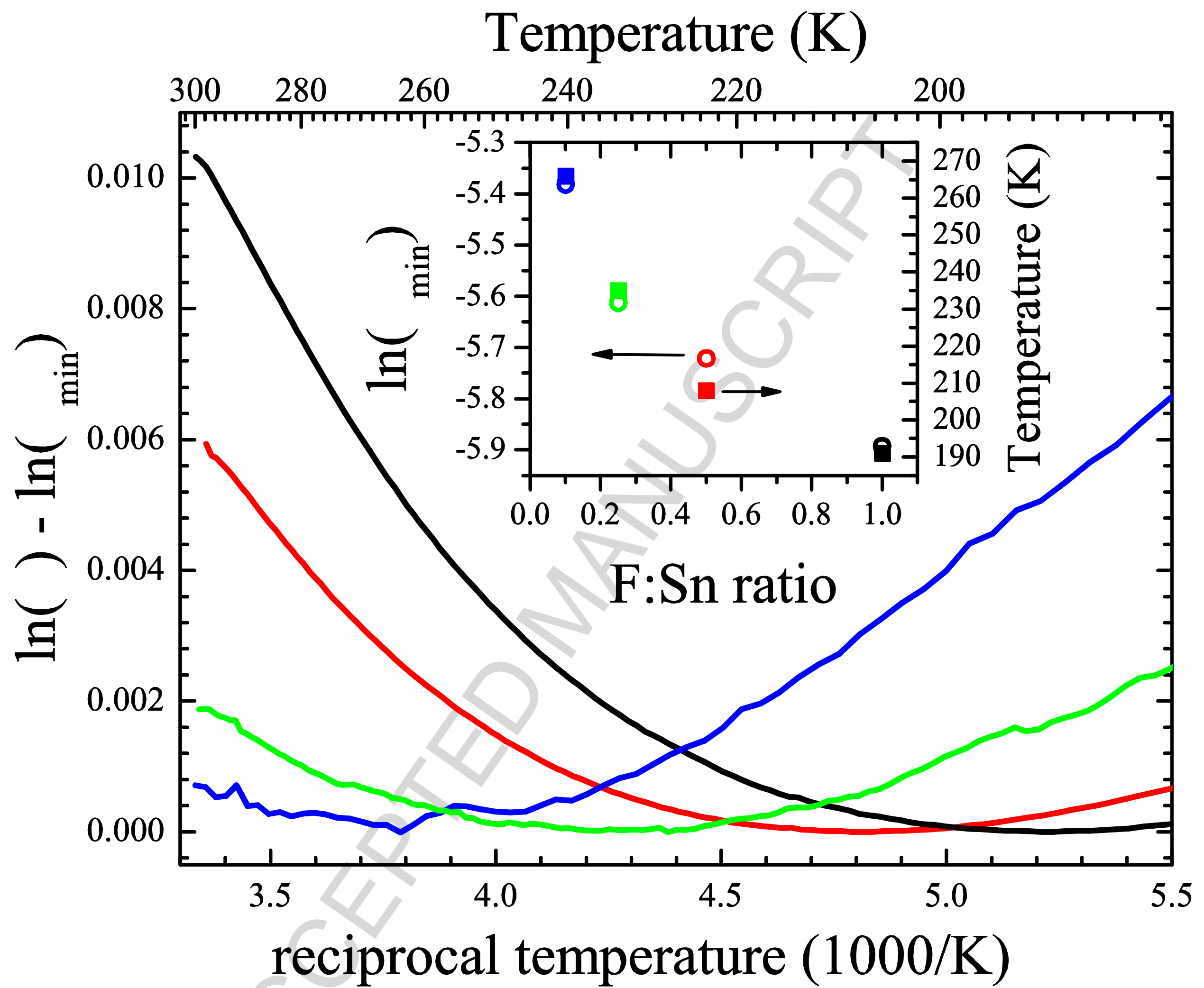

Fig. 5

ACCEPTED MANUSCRIPT

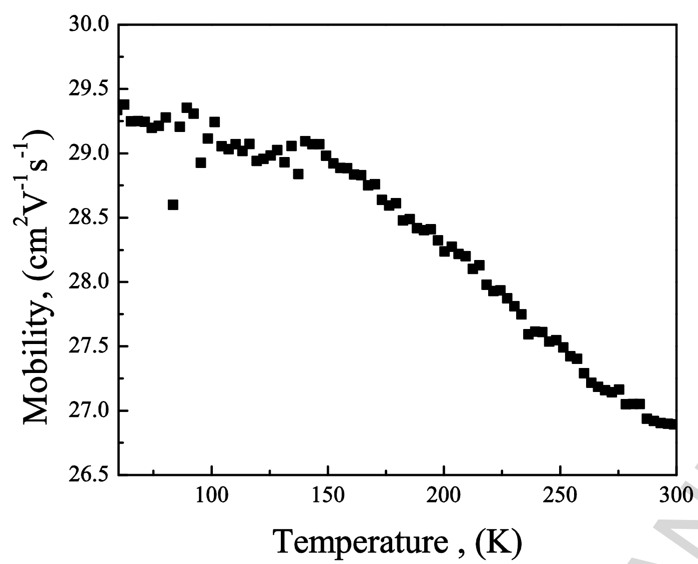

Fig. 6

ACCEPTED MANUSCRIPT

ACCEPTED MANUSCRIPT

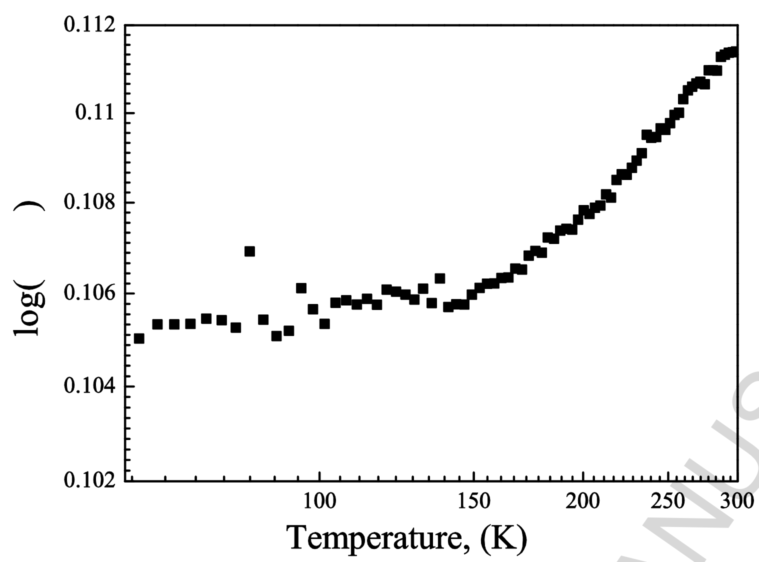

Fig. 7

ACCEPTED MANUSCRIPT